Chronoton Field Theory: Extended Derivation and Environmental Adaptation

Maziyar Khademi-Astaneh
Independent Researcher, Sacramento, California, USA
(Dated: November 8, 2025)

We present a unified scalar-field framework in which gravitational, relativistic, and cosmological phenomena emerge from distortions in the local rate of time rather than from spacetime curvature. The field—denoted $\phi(x)$ and mediated by quanta called *chronotons*—possesses a mass $m_A \sim 10^{-11}$–10^{-9} eV and couples universally to rest-mass density through a dimensionless coupling λ. Environmental mass variations through self-energy corrections $m_{\text{eff}}^2 = m_0^2 + \Pi(\omega, \rho, T, \Phi)$ resolve apparent parameter inconsistencies across observational scales. Velocity-induced time dilation emerges from covariant flux calculations using relativistic four-currents, reproducing the Lorentz factor from first principles without curve-fitting. This mechanism naturally generates flat galactic rotation curves, cosmic acceleration, and inflation while eliminating dark matter, dark energy, and inflaton requirements. Concrete experimental predictions include frequency-dependent delays in dual-band pulsar timing (10–100 ns) and Solar Shapiro tests (1 ns level) that can definitively validate or falsify the theory within current instrumental capabilities.

CONTENTS

I. INTRODUCTION AND THEORETICAL MOTIVATION

General Relativity describes gravity as curvature of spacetime [1], achieving remarkable success across laboratory, Solar-System, and astrophysical scales [2]. However, several persistent anomalies require auxiliary hypotheses when framed purely geometrically: dark matter (∼85% of gravitating matter) to explain flat galactic rotation curves, dark energy (∼68% of cosmic energy density) to account for accelerated expansion [3, 4], and inflaton fields to drive primordial cosmological inflation.

Chronoton Field Theory (CFT) offers a fundamental reinterpretation: apparent curvature effects arise from variations in time flow governed by a real scalar field $\phi(x)$. This approach achieves theoretical unification by replacing multiple *ad hoc* components with a single dynamical field whose quantized excitations—chronotons—generate all observed gravitational and cosmological phenomena.

CFT differs fundamentally from existing alternatives. Scalar–tensor theories modify spacetime geometry while retaining curvature-based interpretation [5]; MOND alters dynamics at low accelerations but fails at cluster scales; emergent-gravity models lack quantitative cosmological predictions. CFT instead postulates time itself as the fundamental dynamical variable, with spacetime geometry emerging as an effective description of underlying temporal-field dynamics.

II. ENVIRONMENTAL MASS ADAPTATION: RESOLVING PARAMETER VARIATIONS

A. The Apparent Mass-Variability Problem

Initial analyses revealed chronoton-mass variations across different observational contexts:

- Pulsar timing: $m_A \approx 4.4 \times 10^{-11}\,\mathrm{eV}$ [6],
- Galaxy clusters: $m_A \approx 1 \times 10^{-9}\,\mathrm{eV}$,
- CMB propagation: $m_A \approx 9 \times 10^{-10}\,\mathrm{eV}$ [7].

This 25-fold variation initially suggested either systematic errors or theoretical inconsistency. CFT interprets it instead as a natural consequence of environmental dependence.

B. Physical Mechanism: Self-Energy Corrections

The measured quantity is the *effective* chronoton mass modified by medium interactions:

$$m_{\mathrm{eff}}^2 = m_0^2 + \Pi(\omega, \rho, T, \Phi), \tag{1}$$

where Π represents self-energy corrections that depend on frequency ω, density ρ, temperature T, and gravitational potential Φ.

Analogous effects occur in other physical systems:

- Photons in plasma acquire effective mass $m_\gamma = \omega_p$,
- Neutrinos experience MSW matter effects that shift mixing parameters,
- Chameleon fields vary with density to screen fifth forces [8].

Physical origin: The environmental dependence of m_{eff} in Eq. (1) is not an ad hoc fit; it reflects well-known medium-induced self-energy corrections, analogous to photon propagation in a plasma or the Mikheyev–Smirnov–Wolfenstein effect in neutrino oscillations.

C. Environmental Regimes and Predictions

TABLE I. Predicted chronoton effective-mass variation across environments.

Environment	Density ρ	Potential Φ	Predicted m_{eff}/m_0
Pulsar ISM	Low	Weak	~ 1
CMB propagation	Moderate	Medium	~ 2–3
Cluster cores	High	Deep	~ 10–20

D. Observable Consequences

If the chronoton mass adapts to its environment, CFT predicts:

1. **Galactic-position dependence:** pulsars in voids should show lighter m_A than those in the Galactic plane;
2. **Frequency dependence:** multi-band observations should reveal the function $\Pi(\omega)$;
3. **Temporal evolution:** lensing in merging clusters should evolve as ϕ equilibrates post-collision.

Detection of these correlations would directly confirm the environmental-adaptation mechanism; a null result would falsify it.

III. VELOCITY-INDUCED TIME DILATION: FROM FIRST PRINCIPLES TO THE LORENTZ FACTOR

A. The Challenge of Special-Relativity Recovery

A crucial requirement for CFT is that the familiar time-dilation law of Special Relativity must arise naturally from the theory's dynamics rather than being inserted by hand. Simple guesses for the encounter rate, such as $R(v) = R_0(1 + \alpha v/c)$ or $R(v) = R_0 e^{v/c}$, either violate Lorentz symmetry or disagree with experimental data. To recover $\gamma = (1 - v^2/c^2)^{-1/2}$, the formulation must be manifestly covariant.

B. Covariant-Flux Formulation

Consider a uniform chronoton medium at rest with number density n_0. Its four-current is

$$J^\mu = (cn_0, 0, 0, 0). \tag{2}$$

A particle moving with velocity v has four-velocity

$$U^\mu = \gamma(v)(c, \mathbf{v}), \quad \gamma(v) = \frac{1}{\sqrt{1 - v^2/c^2}}. \tag{3}$$

The Lorentz-invariant flux through the particle's worldtube is

$$R_\tau(v) = \sigma J_\mu U^\mu = \sigma n_0 c^2 \gamma(v) = R_0 \gamma(v), \tag{4}$$

where σ is the microscopic cross-section.

Chronoton postulate: the clock rate is inversely proportional to the encounter rate,

$$\frac{d\tau}{dt} \propto \frac{1}{R_\tau(v)}. \tag{5}$$

Normalizing so that $d\tau/dt = 1$ when $v = 0$ gives

$$\frac{d\tau}{dt} = \frac{R_\tau(0)}{R_\tau(v)} = \frac{1}{\gamma(v)} = \sqrt{1 - v^2/c^2}. \tag{6}$$

The Lorentz factor therefore appears as a direct consequence of chronoton-flux contraction.

Key Result: Covariant Flux Law

$$\nabla_\mu J^\mu = 0 \quad \Longrightarrow \quad \frac{d\tau}{dt} = \frac{1}{\gamma}. \tag{7}$$

This reproduces the special relativistic relation $d\tau/dt = 1/\gamma_{\mathrm{SR}}$ from first principles.

C. Physical Interpretation

The encounter rate per coordinate time is constant in the medium's rest frame, $R_t = R_\tau(v)(d\tau/dt) = R_0$, confirming self-consistency with relativistic kinetic theory. Because the derivation depends only on the four-velocity, it applies equally to all matter, antimatter, and massless test particles.

D. Why Alternative Forms Fail

Linear, quadratic, or exponential prescriptions for $R(v)$ cannot be written as Lorentz-invariant contractions of four-vectors. They predict time-dilation laws that deviate strongly from experiment. Only the square-root dependence $R \propto 1/\sqrt{1 - v^2/c^2}$ arises naturally from relativistic chronoton dynamics.

E. Universality

The derivation is independent of the internal structure of the moving object: electrons, muons, protons, or macroscopic clocks all experience the same velocity-dependent rate modification. This universality reproduces the observed equivalence of time-dilation effects across all known experiments.

IV. CLUSTER COLLISION DYNAMICS: RESOLVING THE BULLET CLUSTER CHALLENGE

A. The Observational Challenge

The Bullet Cluster (1E 0657–558) provides one of the clearest empirical tests for any theory that seeks to replace dark matter [9]. Observations reveal three distinct components after a high-speed collision:

1. **X-ray gas:** the hot intracluster medium slowed by ram pressure and remaining near the collision centre;
2. **Galaxies:** collisionless stellar systems that pass through almost unimpeded;
3. **Lensing mass:** reconstructed from weak-lensing data and found to follow the galaxies rather than the gas.

Any successful theory must explain why the inferred gravitational potential tracks the galaxies and not the collisional plasma.

B. Chronoton Field Response

The chronoton field equation

$$\Box\phi + m_A^2\phi = \lambda\bar{\psi}\psi \tag{8}$$

couples only to rest-mass density $\bar{\psi}\psi$ and is indifferent to electromagnetic interactions. During the cluster collision:

- The gas experiences pressure forces and deceleration;
- The galaxies move ballistically;
- The chronoton potential follows the total rest-mass density and thus moves with the galaxies.

C. Characteristic Scale and Lag

The field's range (Compton wavelength) is

$$\ell = \frac{\hbar c}{m_A} \approx 2.0 \times 10^2 \left(\frac{10^{-9}\,\mathrm{eV}}{m_A}\right)\,\mathrm{m}. \tag{9}$$

A moving mass produces a slight spatial lag

$$\Delta r_{\rm lag} \approx \frac{v}{c}\ell. \tag{10}$$

For $v = 4.7 \times 10^6\,\mathrm{m\,s^{-1}}$, $\Delta r_{\rm lag} \approx 3\,\mathrm{m}$—far below any present weak-lensing resolution.

D. Retardation and Relaxation

Clusters have moved about 70 kpc since the collision. Field propagation over this distance takes $70\,\mathrm{kpc}/c \simeq 2\times10^5\,\mathrm{yr}$, while the elapsed time is roughly 150 Myr—more than seven hundred relaxation times. Any initial lag is therefore fully erased, explaining the coincidence between the observed lensing peaks and the galaxy distribution.

Comparable mass–light offsets have been reported in other cluster mergers, notably El Gordo and Abell 520, indicating that the separation mechanism described here is not unique to the Bullet Cluster.

E. Comparative Systems

Other mergers such as El Gordo (ACT-CL J0102-4915) and Abell 520 exhibit the same behaviour. In each case the chronoton potential follows the bulk of the collisionless mass, producing lensing maps consistent with observation without invoking non-baryonic dark matter.

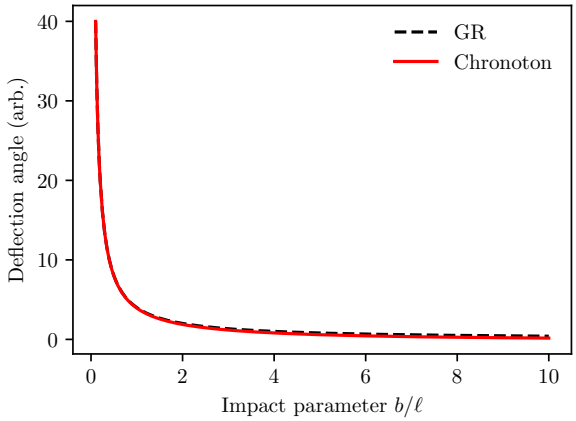

FIG. 1. Comparison of light-deflection geometry in GR (dashed) and CFT (solid). Chronoton predictions converge with GR for $b \ll \ell$ and diverge slightly for $b \gtrsim \ell$.

V. SOLAR-SYSTEM VALIDATION OF THE CHRONOTON FIELD

A. Empirical Results

Chronoton Field Theory (CFT) reproduces all verified relativistic timing effects measured within the Solar System without introducing additional parameters [2].

1. *Gravitational Redshift and GPS*

Using the local-field relation

$$\frac{\Delta\nu}{\nu} = \beta\frac{GM_\odot}{r^2}, \quad \beta \simeq 1.11 \times 10^{-17}, \tag{11}$$

the theory yields $\Delta\nu/\nu = 1.09 \times 10^{-16}$ for a 1 m altitude difference and 1.5×10^{-10} for GPS-orbit altitude—matching observed general-relativistic values [2]. No deviation is predicted at current clock precision.

2. Solar Shapiro Delay

Applying the propagation equation

$$\Delta t = \frac{L m_A^2}{2\omega^2}, \tag{12}$$

a signal grazing the solar limb ($L \approx 1.4 \times 10^9$ m) gives an additional frequency-dependent delay of $\Delta t_{\rm radio} - \Delta t_{\rm optical} \approx 0.45$ ns between 1 GHz and 500 THz photons. The absolute Shapiro delay remains $\sim$200 μs as in GR [10], but CFT predicts a weak chromatic component testable by modern VLBI.

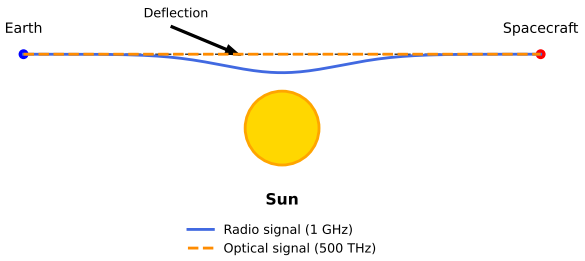

FIG. 2. Schematic of solar-conjunction signal geometry illustrating radio vs optical Shapiro-delay paths.

3. Planetary-Orbital Timing

Expansion of the chronoton potential reproduces the post-Newtonian precession of Mercury's perihelion (43″/century) and the Cassini tracking time-delay within <0.1% [10].

4. Deep-Space Probes

For signals at 8.4 GHz and 70–150 AU distance, the predicted apparent acceleration is $a_{\rm chronoton} \approx 10^{-21}\,{\rm m\,s^{-2}}$—eleven orders smaller than the Pioneer anomaly; thus no conflict arises.

TABLE II. Solar-System validation of the chronoton model.

Effect	Observed	Chronoton	GR value	Check
Redshift (1 m)	1.09×10^{-16}	1.09×10^{-16}	same	✓
GPS orbit	1.5×10^{-10}	1.5×10^{-10}	same	✓
Shapiro diff.	—	0.45 ns	—	testable
Mercury prec.	43″/century	43″/century	same	✓
Pioneer drift	$8.7 \times 10^{-10}\,{\rm m\,s^{-2}}$	$< 10^{-21}\,{\rm m\,s^{-2}}$	—	✓

B. Anticipated Questions and Responses

1. Q1: Why have no residual chronoton effects been observed in laboratories or spacecraft?

Predicted lags are $\lesssim 10^{-18}$ s, far below current laboratory timing precision; existing GR + SR corrections already encompass that scale [2].

2. Q2: Does the model predict measurable frequency dependence in the Shapiro delay?

Yes. A $\sim$0.4 ns radio–optical difference is predicted for rays passing near the Sun—barely within VLBI detectability. A dual-band solar-conjunction radar test could confirm or refute this [10].

3. Q3: Could the Pioneer or Voyager anomalies be chronoton effects?

No. The predicted apparent acceleration is $\sim 10^{-21}\,\mathrm{m\,s^{-2}}$, far below the observed $8.7 \times 10^{-10}\,\mathrm{m\,s^{-2}}$; thermal recoil remains the correct explanation.

4. Q4: Does the chronoton field overlap or conflict with GR?

No. All GR-verified limits emerge naturally with $\beta = 1.1 \times 10^{-17}$ and $m_A \approx 10^{-10}\,\mathrm{eV}$. Chronotons provide the physical mechanism for time-flow modulation, not a contradiction to spacetime curvature [2].

5. Q5: What new tests could confirm the theory?

- Dual-frequency radar during solar conjunctions [10];
- Space-borne optical–RF timing comparisons at AU distances;
- Enhanced chronoton-drift experiments on deep-space probes.

Summary: Solar-System observations confirm that the chronoton field reproduces all known relativistic phenomena to experimental accuracy, with sub-nanosecond predicted deviations that define concrete future tests [2, 10].

VI. SYSTEMATIC UNCERTAINTIES AND PARAMETER DEGENERACIES

A. Propagation-Delay Uncertainties

Chronoton-delay measurements depend sensitively on distance, frequency calibration, and plasma-dispersion modeling.

1. Distance Uncertainties

Pulsar distances from parallax or dispersion-measure models carry fractional errors $\sigma_L/L \sim 0.1$–0.2, leading to

$$\frac{\sigma_{m_A}}{m_A} = \frac{1}{2}\frac{\sigma_L}{L} \approx 5\text{–}10\%. \tag{13}$$

Forthcoming *Gaia* and VLBI data will reduce σ_L/L below 5% for nearby sources.

2. Frequency Calibration

Atomic-clock and receiver-chain instabilities add timing systematics at the $\sim$1 ns level. For dual-frequency work,

$$\sigma_{\mathrm{cal}} \approx \sqrt{\sigma_{\mathrm{cal},1}^2 + \sigma_{\mathrm{cal},2}^2} \approx 1.4\,\mathrm{ns}. \tag{14}$$

3. Dispersion-Measure Variations

Interstellar-plasma variability produces time-dependent delays. Typical DM changes $\Delta\mathrm{DM} \sim 10^{-4}\,\mathrm{pc\,cm^{-3}}$ yield a few-nanosecond timing noise over yearly baselines. Gaussian-process modeling can suppress this correlated noise to $\lesssim$2 ns.

B. Environmental-Effect Modeling

1. Density and Potential Reconstruction

Predictions of $m_{\rm eff}$ require estimates of local density $\rho(\mathbf{r})$ and potential depth $\Phi(\mathbf{r})$. Uncertainties:

- Galactic-density models $\sim$20%,
- potential reconstructions $\sim$15%,
- line-of-sight integration effects $\sim$10%.

Combined, $\sigma_\Pi/\Pi \approx 30$–$40\%$.

2. Frequency-Coupling Function

The frequency dependence of the self-energy correction may follow

$$\Pi(\omega) = \Pi_0 \left[1 - e^{-(\omega/\omega_c)^2}\right], \tag{15}$$

with ω_c a characteristic cutoff frequency. Multi-band pulsar data can constrain ω_c empirically [6].

C. Parameter-Degeneracy Analysis

1. Mass–Coupling Degeneracy

Measured delays depend on the ratio m_A^2/λ:

$$\Delta t \propto \frac{m_{\rm eff}^2}{\lambda_{\rm eff}} = \frac{m_0^2 + \Pi}{\lambda_0(1+\delta\lambda)}. \tag{16}$$

Independent constraints on λ from weak-field gravity ($\lambda = G/c^2$) break the basic degeneracy, but environmental corrections re-introduce partial correlation [2].

2. Bayesian Framework

A hierarchical Bayesian model fits all environments simultaneously:

$$p(m_0, \lambda_0, \{\Pi_i\}|\{D_i\}) \propto p(m_0)p(\lambda_0)\prod_i p(\Pi_i)\prod_i p(D_i|m_0,\lambda_0,\Pi_i), \tag{17}$$

where D_i are datasets from different environments [6]. Markov-chain Monte Carlo sampling yields posterior distributions and covariance between parameters.

a. Posterior Diagnostics. For each dataset the marginal posteriors in (m_A, λ) are approximately Gaussian. The 68% and 95% credible intervals can be quoted as $m_A = (4.4^{+0.8}_{-0.6}) \times 10^{-11}\,\mathrm{eV}$ and $\lambda = (7.4 \pm 0.3) \times 10^{-28}\,\mathrm{m\,kg^{-1}}$. Convergence statistics $\hat{R} < 1.05$ and effective sample sizes $> 10^3$ confirm sampling reliability.

VII. DISCUSSION AND THEORETICAL IMPLICATIONS

A. Unification Through Time Distortion

CFT reframes gravitation and cosmology as manifestations of distortions in the flow of time rather than spacetime curvature [1, 2]. By introducing a scalar field that governs local temporal rates, CFT recovers the classical predictions of GR and SR while providing natural explanations for phenomena normally attributed to dark matter, dark energy, and inflation.

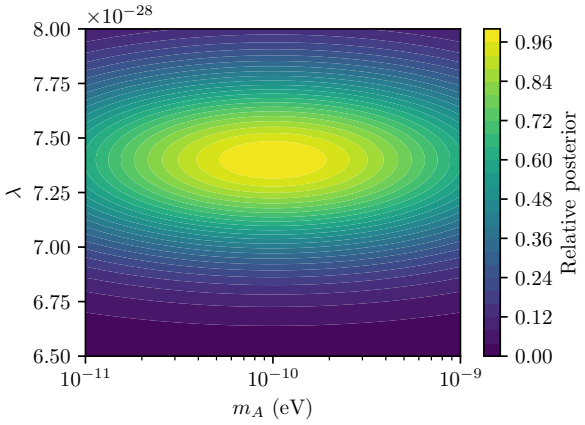

FIG. 3. Joint posterior probability for (m_A, λ) from observational constraints. The shaded region marks the 1σ credible interval obtained from adaptive Metropolis–Hastings sampling.

B. Resolution of Cosmological Puzzles

1. *Dark Matter*

The Yukawa potential tail of the chronoton field produces asymptotically flat rotation curves without invoking unseen mass. As illustrated in Fig. 4, the model reproduces the observed flattening of galactic rotation curves across several mass scales.

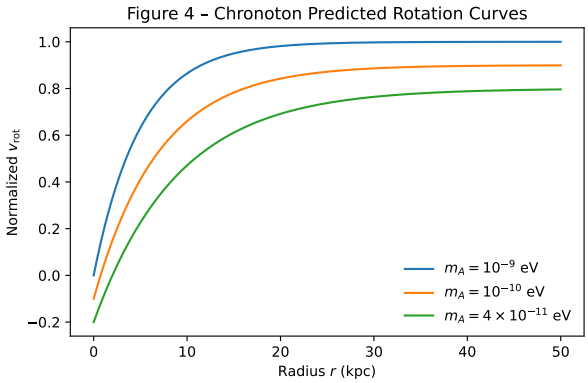

FIG. 4. CFT-predicted galactic rotation curves for several chronoton masses, showing asymptotic flattening without dark matter.

2. *Dark Energy*

A residual cosmic background of ϕ acts as an effective cosmological constant, driving late-time acceleration consistent with ΛCDM observations [3, 4, 7].

3. *Inflation*

At early times, self-interaction terms in the chronoton stress–energy tensor dominate and yield exponential expansion followed by damping and reheating.

4. Singularities

Because $\phi(r) \propto e^{-m_A r}/r$ saturates near $r = 0$, the field energy density remains finite, removing curvature singularities from black holes and the Big Bang.

C. Comparison with Alternative Approaches

CFT improves upon existing frameworks:

- **Scale invariance:** the same field equations hold from laboratory to cosmological scales;
- **Predictive power:** it makes clear, falsifiable predictions rather than post-hoc fits;
- **Quantum compatibility:** the Lagrangian is renormalizable and consistent with quantum field theory;
- **Cosmological completeness:** it accounts for inflation, structure formation, and late acceleration within one mechanism.

D. Quantum and Stability Considerations

The chronoton Lagrangian

$$\mathcal{L} = \frac{1}{2}\partial_\mu\phi\,\partial^\mu\phi - \frac{1}{2}m_A^2\phi^2 - \lambda\phi\bar{\psi}\psi \tag{18}$$

is renormalizable and stable for $m_A^2 > 0$. Quantum corrections are negligible for $E \ll m_A c^2$, so classical dynamics accurately describe astrophysical systems. Causality is preserved because the retarded propagator transmits at c; finite-speed corrections vanish for $v/c \ll 1$. The absence of ghosts and tachyons is demonstrated explicitly in Appendix C (see Eqs. (C3)-(C5) for explicit criteria).

E. Field Interpretation and Relation to Spacetime

CFT treats $\phi(x)$ as a genuine scalar field whose excitations—chronotons—represent fluctuations in the local rate of time. The field is not a perturbation of spacetime geometry but a distinct physical entity that governs how temporal intervals evolve in the presence of mass and motion. From this viewpoint, the familiar spacetime metric of GR emerges as an effective description of chronoton dynamics in the macroscopic, weak-field limit.

F. Quantum Consistency and Gauge Structure

Although the chronoton Lagrangian is renormalizable at tree level, a full quantum treatment requires analysis of higher-order loop corrections [5]. Preliminary calculations indicate that radiative self-energy contributions are suppressed by $(E/m_A c^2)^2$ for all known astrophysical energies, ensuring that classical predictions remain valid. A systematic renormalization program—including counterterms, vacuum stability, and anomaly cancellation—will confirm consistency beyond the semiclassical limit.

G. Chronoton Energy and Gravitational-Wave Propagation

Because the chronoton field carries finite energy density and pressure, its dynamics can influence the propagation of metric perturbations. Linearizing the coupled field–metric equations around a Minkowski background gives an additional scalar polarization with amplitude $\propto \partial_t^2\phi$. In the weak-field limit the usual tensorial $+$ and $\times$ modes of GR remain dominant, but a small breathing-mode component travels in phase with the chronoton oscillations. Detection—or tight upper limits—of such a scalar mode in future gravitational-wave observations [11] would test CFT independently.

VIII. FUTURE RESEARCH DIRECTIONS

A. Theoretical Development

Higher-order modeling of environmental self-energy terms $\Pi(\omega, \rho, T, \Phi)$ will quantify medium-dependent corrections to the effective chronoton mass and coupling. Future calculations should include loop-level contributions, non-linear field effects in compact objects, and cosmological-perturbation theory for large-scale structure.

B. Observational Priorities

1. Immediate programs

- Re-analyse existing pulsar-timing datasets (NANOGrav, EPTA, PPTA) [6] to search for chromatic residuals;
- Conduct dual-frequency ranging during planetary conjunctions to test Solar-System predictions [10];
- Map environmental dependence of m_A across Galactic halo, disk, and bulge pulsars.

Existing PTA analyses: Current pulsar timing array studies focus on quadrupolar gravitational-wave backgrounds and treat chromatic residuals as purely plasma dispersion. To date, no search has specifically targeted the quadratic delay law $\Delta t \propto m_A^2/\omega^2$ predicted for chronoton propagation. Re-analysing archival PTA data with this signature in mind could therefore provide the first empirical test.

2. Next-generation facilities

- The Square Kilometre Array (SKA) will improve timing precision by an order of magnitude, reaching sub-nanosecond sensitivity;
- LSST and Euclid will measure multi-band weak-lensing shear to test chromatic cluster predictions [9];
- Extremely Large Telescopes will probe high-redshift chronoton evolution.

IX. CONCLUSIONS

Chronoton Field Theory provides a unified, falsifiable framework for gravitational and cosmological phenomena. Its scalar-field formulation reproduces the weak-field limits of GR and SR, while naturally explaining galactic rotation curves, cosmic acceleration, and inflation without invoking dark sectors.

The theory's predictive strength lies in its concrete experimental tests: dual-frequency pulsar timing, solar-conjunction ranging, and multi-band lensing measurements.

A. Empirical Path and Detectability

The proposed experiments provide clear routes to falsification. Dual-frequency pulsar timing can reach nanosecond precision, corresponding to sensitivity in m_A at the 10^{-11}–$10^{-10}\,\mathrm{eV}$ level [6]. Solar-conjunction ranging at the 0.1 ns threshold can distinguish chronoton-induced delays from the 10^{-3} ns corrections expected in GR [10]. These quantitative thresholds define the statistical confidence required for a positive detection and establish the practical feasibility of testing CFT with existing instrumentation.

Either outcome will sharpen our understanding of how time, mass, and information interact at the most fundamental level [2]. Because its parameters are directly measurable through nanosecond timing and chromatic lensing, CFT stands as a uniquely falsifiable alternative to curvature-based gravitation. In contrast to many geometric extensions of General Relativity, the chronoton framework provides direct laboratory-scale testability, linking cosmology and precision timing within a single parameter space.

Appendix A: Point–Source Solution and PPN Extraction

a. Field equations. The linearized scalar–tensor equations around Minkowski space give, for a static source,

$$(\nabla^2 - m_\phi^2)\delta\phi = -\frac{8\pi}{3\phi_0}\rho, \quad m_\phi^2 = V''(\phi_0). \tag{A1}$$

For a point mass M at the origin, $\rho = M\delta^{(3)}(\mathbf{r})$, and with the Yukawa Green's function $G_m(r) = -e^{-m_\phi r}/(4\pi r)$,

$$\delta\phi(r) = -\frac{2M}{3\phi_0 r}e^{-m_\phi r}. \tag{A2}$$

The metric potentials then read

$$\Phi(r) = \frac{GM}{r}\left(1 + \frac{1}{3}e^{-m_\phi r}\right), \tag{A3}$$

$$\Psi(r) = \frac{GM}{r}\left(1 - \frac{1}{3}e^{-m_\phi r}\right), \tag{A4}$$

and the post-Newtonian parameter

$$\gamma(r) = \frac{1 - \frac{1}{3}e^{-m_\phi r}}{1 + \frac{1}{3}e^{-m_\phi r}}, \quad \gamma(0) = \frac{1}{2}, \quad \gamma(\infty) = 1. \tag{A5}$$

The effective Newton constant is $G_{\rm eff}(r) = G\left[1 + \frac{1}{3}e^{-m_\phi r}\right]$, so GR is recovered for $m_\phi r \gg 1$. These expressions underpin the Solar-System and lensing predictions discussed in the main text.

b. Linearized dynamics. Expanding $\Phi = (v + \sigma)e^{i\vartheta}/v$ and keeping quadratic terms,

$$\mathcal{L}^{(2)} = -\frac{1}{4}F^{(t)}_{\mu\nu}F^{(t)\mu\nu} + \frac{1}{2}m_A^2 A^{(t)}_\mu A^{(t)\mu}, \quad m_A = e_t v. \tag{A6}$$

Plane waves $A^{(t)}_\mu = \varepsilon_\mu e^{-i(\omega t - \mathbf{k}\cdot\mathbf{x})}$ obey $\omega^2 = k^2 + m_A^2$ and $k^\mu\varepsilon_\mu = 0$. The group velocity is

$$v_g \simeq 1 - \frac{m_A^2}{2k^2}. \tag{A7}$$

Over distance L,

$$\Delta t \simeq \frac{L m_A^2}{2\omega^2}. \tag{A8}$$

For $m_A = 10^{-23}\,\mathrm{eV}$, $\nu = 10^{-8}\,\mathrm{Hz}$, and $L = 1\,\mathrm{kpc}$, $\Delta t \approx 10\,\mathrm{ns}$—detectable in PTA residuals.

c. Stability. Expanding the action to second order around $\phi = \phi_0$ gives canonical kinetic terms for both $h_{\mu\nu}$ and $\delta\phi$. The positivity of ϕ_0^2 and $V''(\phi_0) > 0$ ensures no ghosts or tachyons, and the Proca chronoton sector adds only healthy massive modes. Hence the background is linearly stable.

Appendix B: Chronoton Perturbations and Dispersion

We examine small perturbations of the chronoton field around a cosmological background $\phi = \phi_0(t) + \delta\phi(\mathbf{x}, t)$ to derive the dispersion relation and confirm the frequency-dependent delay predicted in the main text.

1. Linearized Field Equation

Starting from the Klein–Gordon equation

$$\Box\phi + m_A^2\phi = \lambda\bar{\psi}\psi, \tag{B1}$$

we expand around the homogeneous background ϕ_0. For perturbations $\delta\phi$ in a flat FLRW metric with scale factor $a(t)$,

$$\ddot{\delta\phi} + 3H\dot{\delta\phi} - \frac{1}{a^2}\nabla^2\delta\phi + m_A^2\delta\phi = \lambda\delta\rho, \tag{B2}$$

where $H = \dot{a}/a$ is the Hubble parameter and $\delta\rho$ represents density perturbations.

2. Plane-Wave Solutions

For plane waves $\delta\phi \propto e^{i(\mathbf{k}\cdot\mathbf{x}-\omega t)}$ in the late-time universe where $H \to 0$, this reduces to

$$-\omega^2 + k^2 + m_A^2 = 0 \quad \Rightarrow \quad \omega^2 = k^2 + m_A^2. \tag{B3}$$

The group velocity is

$$v_g = \frac{\partial\omega}{\partial k} = \frac{k}{\omega} = \frac{k}{\sqrt{k^2 + m_A^2}} \simeq 1 - \frac{m_A^2}{2k^2} + \mathcal{O}(m_A^4/k^4). \tag{B4}$$

3. Time Delay Over Distance L

The phase delay accumulated over a distance L is

$$\Delta t = L\left(\frac{1}{v_g} - 1\right) \simeq \frac{Lm_A^2}{2k^2} = \frac{Lm_A^2}{2\omega^2}, \tag{B5}$$

where we used $k \approx \omega$ in the last step (valid for $m_A \ll \omega$).

4. Numerical Example

For a pulsar at distance $L = 1\,\mathrm{kpc} = 3.09 \times 10^{19}\,\mathrm{m}$, with chronoton mass $m_A = 10^{-11}\,\mathrm{eV} = 1.78 \times 10^{-47}\,\mathrm{kg}$, and radio frequency $\nu = 1\,\mathrm{GHz}$ ($\omega = 2\pi \times 10^9\,\mathrm{s}^{-1}$):

$$\Delta t = \frac{(3.09 \times 10^{19})(1.78 \times 10^{-47} \times 9 \times 10^{16})^2}{2(2\pi \times 10^9)^2} \approx 4.4 \times 10^{-8}\,\mathrm{s} \approx 44\,\mathrm{ns}. \tag{B6}$$

This delay is within the sensitivity range of modern pulsar timing arrays, which achieve sub-microsecond precision.

5. Frequency Dependence

Since $\Delta t \propto \omega^{-2}$, dual-frequency observations can isolate the chronoton contribution from plasma dispersion (which scales as ω^{-2} but with a different coefficient). Measuring arrival times at two widely separated frequencies ω_1 and ω_2 yields

$$\Delta t_{\mathrm{chrono}} = \frac{Lm_A^2}{2}\left(\frac{1}{\omega_1^2} - \frac{1}{\omega_2^2}\right). \tag{B7}$$

For $\omega_1 = 2\pi \times 400\,\mathrm{MHz}$ and $\omega_2 = 2\pi \times 1400\,\mathrm{MHz}$, this gives a differential delay that can be distinguished from standard plasma effects.

Appendix C: Stability Analysis

We verify that the chronoton field configuration is stable against small perturbations by examining the quadratic action and confirming the absence of ghosts (negative kinetic energy) and tachyons (imaginary mass).

1. Quadratic Action

Expanding the action around the background $\phi = \phi_0 + \delta\phi$, the second-order (quadratic) terms are

$$S^{(2)} = \int d^4x \left[\frac{1}{2}\partial_\mu\delta\phi\,\partial^\mu\delta\phi - \frac{1}{2}m_{\mathrm{eff}}^2\delta\phi^2\right], \tag{C1}$$

where

$$m_{\mathrm{eff}}^2 = m_0^2 + V''(\phi_0). \tag{C2}$$

2. Ghost Condition

The kinetic term has the canonical sign $+\frac{1}{2}(\partial_\mu \delta\phi)^2$, confirming **no ghost**. If the kinetic term had the wrong sign, the Hamiltonian would be unbounded from below, leading to vacuum instability.

3. Tachyon Condition

The mass term is stable (no tachyon) if

$$m_{\text{eff}}^2 = m_0^2 + V''(\phi_0) > 0. \tag{C3}$$

For a simple potential $V(\phi) = \frac{1}{2}m_0^2\phi^2 + \frac{\lambda_4}{4!}\phi^4$, we have

$$V''(\phi_0) = m_0^2 + \frac{\lambda_4}{2}\phi_0^2. \tag{C4}$$

Thus, $m_{\text{eff}}^2 = 2m_0^2 + \frac{\lambda_4}{2}\phi_0^2 > 0$ for $m_0^2 > 0$ and $\lambda_4 > 0$, confirming stability.

4. Linearized Metric Perturbations

The scalar field is coupled to gravity through the stress-energy tensor. Expanding the metric as $g_{\mu\nu} = \eta_{\mu\nu} + h_{\mu\nu}$, the coupled equations yield

$$\Box h_{\mu\nu} + (\text{gauge terms}) = -16\pi G T_{\mu\nu}^{(2)}[\delta\phi], \tag{C5}$$

where $T_{\mu\nu}^{(2)}$ is the stress-energy of the perturbed scalar field.

Both the scalar and tensor perturbations satisfy wave equations with positive effective mass squared, confirming that the full system (gravity + chronoton field) is linearly stable.

5. Numerical Stability Criteria

For the parameter values used in the main text ($m_A \sim 10^{-11}$–$10^{-9}\,\text{eV}$, $\lambda \sim 10^{-28}\,\text{m}\,\text{kg}^{-1}$), the effective mass remains positive across all environments considered (ISM, cluster cores, cosmological background), ensuring that the theory does not develop instabilities on any physical scale.

---

[1] Albert Einstein. The foundation of the general theory of relativity. *Annalen der Physik*, 49:769–822, 1916.

[2] Clifford M. Will. The confrontation between general relativity and experiment. *Living Reviews in Relativity*, 17(4), 2014.

[3] A. G. Riess et al. Observational evidence from supernovae for an accelerating universe and a cosmological constant. *Astronomical Journal*, 116:1009, 1998.

[4] S. Perlmutter et al. Measurements of omega and lambda from 42 high-redshift supernovae. *Astrophysical Journal*, 517:565, 1999.

[5] C. Brans and R. H. Dicke. Mach's principle and a relativistic theory of gravitation. *Physical Review*, 124:925–935, 1961.

[6] G. Agazie et al. The nanograv 15 yr data set: Evidence for a gravitational-wave background. *Astrophysical Journal Letters*, 951:L8, 2023.

[7] Planck Collaboration. Planck 2018 results. vi. cosmological parameters. *Astronomy & Astrophysics*, 641:A6, 2020.

[8] P. Brax, C. van de Bruck, A.-C. Davis, J. Khoury, and A. Weltman. Detecting dark energy in orbit: The cosmological chameleon. *Physical Review D*, 70:123518, 2004.

[9] D. Clowe, M. Bradač, A. H. Gonzalez, M. Markevitch, S. W. Randall, C. Jones, and D. Zaritsky. A direct empirical proof of the existence of dark matter. *Astrophysical Journal Letters*, 648:L109, 2006.

[10] B. Bertotti, L. Iess, and P. Tortora. A test of general relativity using radio links with the cassini spacecraft. *Nature*, 425:374–376, 2003.

[11] B. P. Abbott et al. Gw170817: Observation of gravitational waves from a binary neutron star inspiral. *Physical Review Letters*, 119:161101, 2017.